Hybrid Transmission Scheme for Improving Link Reliability in mmWave URLLC Communications

Paul Ushiki Adamu, Miguel López-Benítez, *Senior Member, IEEE*, and Jiayi Zhang, *Senior Member, IEEE*

***Abstract*—Ultra-Reliable and Low-Latency Communication (URLLC) represents a key ingredient of current 5G and future 6G mobile communication networks. The demanding reliability requirement set for URLLC claims for novel techniques that can deliver the necessary level of reliability without sacrificing the overall system capacity. In this context, this work presents and analyses a hybrid transmission scheme for improved reliability in millimetre wave bands with adaptive diversity combining. The proposed scheme is based on a hybrid approach that combines two links, one in the FR1 band (characterised by lower capacity but higher reliability due to more favourable propagation) and one in the FR2 band (offering higher capacity but experiencing a less reliable connectivity). The proposed scheme dynamically adapts the usage of both links in order to exploit the complementary characteristics of both bands (reliability of FR1 bands and capacity of FR2 bands) by switching between FR2-only and joint FR1-FR2 transmission according to the instantaneous channel quality in the main FR2 link. The performance is evaluated under two popular and well-known diversity combining techniques, namely Selection Combining (SC) and Maximal Ratio Combining (MRC). The obtained results demonstrate that the proposed scheme can achieve the same level of reliability as a continuous dual-link transmission scheme but with a much lower level of links usage and without sacrificing (and indeed enhancing) the capacity, thus making it a suitable candidate to deliver URLLC services in a resource-efficient manner.**

***Index Terms*—5G new radio, ultra-reliable low-latency communication, millimetre wave communication, diversity receivers.**

I. Introduction

A key distinguishing feature of the 5th Generation (5G) of cellular mobile communication systems with respect to its predecessors is the introduction of three generic use cases or connectivity types: enhanced Mobile BroadBand (eMBB), massive Machine-Type Communication (mMTC) and Ultra-Reliable Low-Latency Communication (URLLC). The interest of this research is in the URLLC use case, which is related to applications such as the communication among machines and robots for the monitoring, control and automation of industrial processes in the context of the Industry 4.0 paradigm, automotive scenarios in Intelligent Transportation Systems (ITS), tactile Internet, remote healthcare, mission-critical services and ad-hoc disaster/emergency relief among others [1]–[3].

The three use cases, also relevant in 6G, are characterised by vastly heterogeneous and often mutually conflicting requirements. For URLLC, a general reliability requirement of $1 - 10^{-5}$ (i.e., 99.999%) with a user plane latency below 1 ms is specified in [4]. This high reliability requirement makes the wireless access design very challenging in terms of protocols and associated transmission techniques [5]–[7]. The main problem addressed in this work is how to improve the link reliability in order to meet as closely as possible the strict reliability requirements set for URLLC services.

With the aim to enable URLLC, a broad range of techniques have been proposed at the physical [8]–[10], link [11]–[17] and network [18]–[20] layers. However, given the existence of system trade-offs [21], the introduction of techniques to improve the reliability and latency of URLLC services reduces the capacity available for eMBB [22], which has motivated the development of solutions specifically designed to handle eMBB/URLLC coexistence scenarios [23]–[26]. The main challenge is how to improve the link reliability without sacrificing the overall system capacity. Most solutions proposed so far in the literature to improve the link reliability achieve their objective at the expense of sacrificing the system capacity quite significantly. The trade-off between the conflicting interests of eMBB and URLLC services (capacity vs. reliability/latency) is efficiently addressed by the technique proposed in this work.

A well-known strategy to improve the communication reliability is to create simultaneous connections over multiple communication paths and transmit over them in parallel to achieve redundancy. This concept, referred to as Multi-Connectivity (MC), has been paid significant attention as a promising technique not only to increase the system capacity but also to effectively achieve high reliability in URLLC [27]. As a result, different MC techniques have been introduced in successive 3GPP releases in the PHY (e.g, coordinated multi-point), MAC (e.g., carrier aggregation), PDCP (e.g., dual connectivity and LTE-WiFi aggregation) and higher layers [27]. While PHY layer MC techniques are usually constrained to transmitting the same data simultaneously over the multiple paths available, MC techniques at the MAC and higher layers can transmit different data streams in each path, which can be scheduled according to various principles such as load balancing, packet duplication and packet splitting [27].

In this context, the solution proposed in this work is a novel PHY layer MC technique based on diversity reception that exploits and benefits from the complementary characteristics of the multiple frequency bands available in 5G New Radio

P. U. Adamu is with the Department of Electrical Engineering and Electronics, University of Liverpool, Liverpool, L69 3GJ, United Kingdom (email: p.u.adamu@liverpool.ac.uk).

M. López-Benítez is with the Department of Electrical Engineering and Electronics, University of Liverpool, Liverpool, L69 3GJ, United Kingdom, and also with the ARIES Research Centre, Antonio de Nebrija University, 28040 Madrid, Spain (email: m.lopez-benitez@liverpool.ac.uk).

J. Zhang is with the School of Electronic and Information Engineering, Beijing Jiaotong University, Beijing 100044, China (e-mail: jiayizhang@bjtu.edu.cn).

Final author version (January 2023).

(NR), which are divided into two frequency ranges. Frequency Range 1 (FR1) includes the sub-6 GHz bands traditionally used by previous mobile communication standards along with some new bands introduced to cover the spectrum from 410 MHz to 7125 MHz [28, Table 5.1-1]. On the other hand, Frequency Range 2 (FR2) embraces millimetre wave (mmWave) bands from 24.25 GHz to 52.6 GHz [29, Table 5.1-1]. Given the limited capacity available in FR1 bands, new FR2 bands were introduced with the aim to meet the capacity requirements of eMBB. The larger bandwidths available in the mmWave spectrum and its comparatively lower level of usage make FR2 bands a preferred choice for the provision of eMBB. However, path loss and signal blockage are more pronounced at higher frequencies, which makes radio propagation in mmWave bands more challenging and gives rise to unstable connectivity and unreliable communication [30]–[32]. To benefit from the complementary characteristics of both bands (i.e., reliability of FR1 bands and capacity of FR2 bands), this work proposes a novel technique for hybrid FR1/FR2 transmission with adaptive combining at the receiver. In the proposed scheme, an FR2 link is used as the main communication link to provide high capacity, whereas an FR1 link is used as a backup to provide improved reliability when needed. As long as the instantaneous Signal-to-Noise Ratio (SNR) in the FR2 link remains above a certain threshold that ensures an acceptable communication quality, the FR2 link is used alone and the FR1 link either remains in standby mode or is used for other data transmissions. However, when the FR2 link quality becomes unacceptable (i.e., its instantaneous SNR falls below a set threshold), the FR1 link is activated and the same signal is transmitted in both FR1 and FR2 links in order to benefit from the increased reliability offered by the FR1 bands (while both links are simultaneously active, a diversity reception technique is used at the receiver). As soon as the signal quality in the FR2 link increases above the threshold, the system switches back to the FR2 link to enjoy the higher data rates available in mmWave bands and puts the FR1 link in standby mode (to save energy and reduce interference to the environment) or employs it for other data transmissions (to increase resource efficiency). This dynamic transmission approach allows the proposed hybrid scheme to simultaneously benefit from the reliability of FR1 bands and the capacity of FR2 bands. Moreover, compared to the static diversity scenario of dual-link transmission where both FR1/FR2 links are used continuously [33], the proposed scheme conserves energy and prevents unnecessary interference to the environment (if the FR1 link is put in standby) or increases resource efficiency (if the FR1 link is also used for other data transmissions).

The contributions of this work are summarised below:

- An analysis of the SNR statistics at the receiver is provided when two popular diversity techniques, namely Selection Combining (SC) and Maximal Ratio Combining (MRC) [34], are employed. These analytical results are useful to derive various important performance metrics.
- Based on the obtained SNR statistics, the probability of outage and the probability of using the FR1 link under both diversity techniques are evaluated as a function of the received signal quality (represented in terms of the communication distance). The optimum configuration of the FR1/FR2 switching threshold that ensures the highest level of communication reliability is determined.
- Analytical expressions are derived and used to evaluate the bit-error performance of the proposed hybrid scheme under SC/MRC diversity for various configurations.
- Finally, analytical expressions are also derived for the ergodic capacity of the proposed scheme under SC/MRC diversity, which are used to evaluate its performance for various configurations and operating conditions.

The obtained analytical, simulation and numerical results demonstrate that the proposed hybrid FR1/FR2 transmission scheme can achieve the same level of reliability (in terms of outage probability and bit-error rate) as the continuous dual-link transmission scheme, however with a significantly lower level of usage of the FR1 link, thus resulting in a much more efficient use of the available spectral resources. Moreover, this high level of link reliability is not obtained at the expense of the link capacity, which is indeed improved by the application of the proposed scheme, thus making it an ideal candidate for URLLC in heterogeneous scenarios with eMBB services.

The remainder of this work is organised as follows. First, Section II presents the system model considered in this work along with the proposed hybrid transmission scheme. Then Section III derives analytical expressions for the SNR statistics at the receiver under both diversity techniques, which are used in Section IV to derive further analytical expressions for the outage probability, FR1 link usage probability, bit-error rate and ergodic capacity of the proposed scheme. The obtained analytical expressions are used in Section V to evaluate the performance of the proposed hybrid transmission technique. The focus of Sections III and IV is on the mathematical analysis of the proposed hybrid transmission scheme rather than the discussion of its behaviour and performance, which is actually presented in Section V along with logic explanations. Finally, Section VI summarises and concludes this work.

II. System Model

As illustrated in Fig. 1, the hybrid transmission system operates over two links in the FR1 (sub-6 GHz) and FR2 (mmWave) bands. The FR1 link is used as a backup for the FR2 link, which is the main communication link and remains always active. The FR1 link will remain in standby mode as long as the instantaneous SNR in the FR2 link, γ_2, is above a certain SNR threshold, γ_T, which is defined as the minimum SNR required to provide the desired link performance, for instance in terms of the Bit Error Rate (BER). When γ_2 falls below γ_T, the receiver sends a feedback signal to the transmitter to activate the FR1 link and transmit simultaneously the same data in both links. The receiver will then employ a diversity technique to combine the information received in both links. As soon as γ_2 increases above γ_T, the receiver sends a feedback signal to the transmitter to deactivate the FR1 link and communication resumes in the FR2 link only.

In this work, two diversity combining techniques (SC and MRC) are considered to combine the signals received in the

FR1 and FR2 links when both links are activated simultaneously. In MRC, the signals in both links are averaged, weighted by their respective channel impulse responses. This diversity technique is known to be optimal since it maximises the effective SNR, which is given by $\gamma_1 + \gamma_2$ [35, eq. (6.22)]. However, MRC requires the knowledge of all channel fading parameters for each individual link, which results in a higher complexity. On the other hand, SC selects the signal with the highest instantaneous SNR, which leads to a much simpler receiver design at the expense of a lower SNR performance, which in this case is given by $\max(\gamma_1, \gamma_2)$ [35, eq. (6.6)]. While other diversity techniques have been proposed in the literature, SC and MRC are selected in this study owing to their popularity and the representative levels of trade-off that they provide between complexity and performance.

In the FR1 link, the instantaneous SNR per symbol, denoted by γ_1, follows a Rayleigh fading process. Its Probability Density Function (PDF) and Cumulative Distribution Function (CDF) are given, respectively, by [34, eq. (2.7)]

$$f_{\gamma_1}(x) = \frac{1}{\overline{\gamma}_1} \exp\left(-\frac{x}{\overline{\gamma}_1}\right), \tag{1}$$

$$F_{\gamma_1}(x) = 1 - \exp\left(-\frac{x}{\overline{\gamma}_1}\right), \tag{2}$$

where $\overline{\gamma}_1$ is the average SNR in the FR1 link. Rayleigh fading is commonly employed in sub-6 GHz bands to model non-line-of-sight conditions and is chosen here for the FR1 link so that any performance improvement shown in this analysis for the proposed scheme corresponds to an unfavourable propagation scenario (i.e., better performance may be achieved in practice).

For the FR2 link, the Fluctuating Two-Ray (FTR) model is more realistic [36]. According to this model, the instantaneous SNR per symbol, γ_2, is distributed as [37, eq. (6)–(8)]

$$f_{\gamma_2}(x) = \frac{m^m}{\Gamma(m)} \sum_{j=0}^{\infty} \frac{K^j d_j}{(j!)^2} \frac{x^j}{(2\sigma^2)^{j+1}} \exp\left(-\frac{x}{2\sigma^2}\right), \tag{3}$$

$$F_{\gamma_2}(x) = \frac{m^m}{\Gamma(m)} \sum_{j=0}^{\infty} \frac{K^j d_j}{(j!)^2} \gamma\left(j+1, \frac{x}{2\sigma^2}\right), \tag{4}$$

where m is the fading severity index, K is the ratio between the average powers in the specular (i.e., dominant) and the diffuse (i.e., scattered) multipath components, $2\sigma^2$ is the total power of the diffuse components, $\Gamma(\cdot)$ is the (standard) gamma function [38, eq. (8.310.1)], $\gamma(\cdot,\cdot)$ is the lower incomplete gamma function [38, eq. (8.350.1)], and d_j is [39, eq. (13)]

$$d_j \triangleq \sum_{k=0}^{j} \binom{j}{k} \left(\frac{\Delta}{2}\right)^k \sum_{l=0}^{k} \binom{k}{l} \frac{\Gamma(j+m+2l-k)}{\left((m+K)^2 - (K\Delta)^2\right)^{\frac{j+m}{2}}} \times (-1)^{2l-k} \; P_{j+m-1}^{k-2l}\left(\frac{m+K}{\sqrt{(m+K)^2 - (K\Delta)^2}}\right), \tag{5}$$

where the parameter $\Delta \in [0,1]$ characterises the similarity of the two dominant waves (for $\Delta = 0$ one of them is zero and for $\Delta = 1$ both are equal) and $P_\nu^\mu(\cdot)$ is the associated Legendre function (or spherical function) of the first kind [38, eq. (8.702)]. An alternative expression for d_j is given by [39, eq. (19)]. In the FTR model, the average SNR is obtained as $\overline{\gamma}_2 = (E_b/N_0)2\sigma^2(1+K)$, where E_b/N_0 is the energy per bit to noise power spectral density ratio.

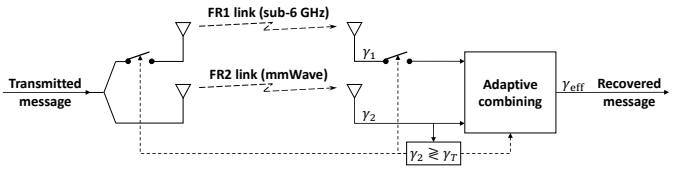

Fig. 1: Proposed hybrid transmission scheme.

III. Analysis of SNR Statistics

A. Cumulative Distribution Function of the SNR

Based on the operation of the proposed hybrid scheme, the instantaneous effective SNR at the receiver, denoted by γ_{eff}, will be equal to γ_2 when $\gamma_2 > \gamma_T$ or the result of combining γ_1 and γ_2 (according to the employed diversity technique) when $\gamma_2 \leq \gamma_T$. Thus, one can write the CDF of the SNR as

$$F_{\gamma_{\text{eff}}}(x) = P\big(g(\gamma_1,\gamma_2) \leq x, \gamma_2 \leq \gamma_T\big) + P\big(\gamma_2 \leq x, \gamma_2 > \gamma_T\big), \tag{6}$$

where $g(\gamma_1,\gamma_2)$ characterises the effective SNR at the output of the selected diversity technique as a function of the SNR for each individual input signal: $g(\gamma_1,\gamma_2) = \max(\gamma_1,\gamma_2)$ for SC [35, eq. (6.6)] and $g(\gamma_1,\gamma_2) = \gamma_1 + \gamma_2$ for MRC [35, eq. (6.22)]. Equation (6) is particularised below for SC and MRC.

Theorem 1 (CDF of SNR under SC)**.** *The CDF of SNR for the proposed hybrid system under SC is given by*

$$F_{\gamma_{\text{eff}}}(x) = \begin{cases} \left[1 - \exp\left(-\frac{x}{\overline{\gamma}_1}\right)\right] \frac{m^m}{\Gamma(m)} & \text{(7a)} \\ \times \sum_{j=0}^{\infty} \frac{K^j d_j}{(j!)^2} \; \gamma\left(j+1, \frac{x}{2\sigma^2}\right), \qquad x \leq \gamma_T, & \\ \frac{m^m}{\Gamma(m)} \sum_{j=0}^{\infty} \frac{K^j d_j}{(j!)^2} \left[\gamma\left(j+1, \frac{x}{2\sigma^2}\right)\right. & \text{(7b)} \\ \left. - \exp\left(-\frac{x}{\overline{\gamma}_1}\right) \gamma\left(j+1, \frac{\gamma_T}{2\sigma^2}\right)\right], \quad x > \gamma_T. & \end{cases}$$

Proof. The expression in (6) can be rewritten in terms of the associated conditional probabilities as

$$F_{\gamma_{\text{eff}}}(x) = P(g(\gamma_1,\gamma_2) \leq x \,|\, \gamma_2 \leq \gamma_T) P(\gamma_2 \leq \gamma_T) \tag{8}$$

$$+ P(\gamma_2 \leq x \,|\, \gamma_2 > \gamma_T) P(\gamma_2 > \gamma_T). \tag{9}$$

When $\gamma_2 \leq \gamma_T$, then $g(\gamma_1,\gamma_2) = \max(\gamma_1,\gamma_2)$ under SC, thus the conditional probability in (8) can be expressed as

$$\begin{aligned} P(g(\gamma_1,\gamma_2) \leq x \,|\, \gamma_2 \leq \gamma_T) &= P(\max(\gamma_1,\gamma_2) \leq x \,|\, \gamma_2 \leq \gamma_T) \\ &= P(\gamma_1 \leq x) P(\gamma_2 \leq x \,|\, \gamma_2 \leq \gamma_T) \\ &= F_{\gamma_1}(x) \cdot \min\left(1, \frac{F_{\gamma_2}(x)}{F_{\gamma_2}(\gamma_T)}\right). \end{aligned} \tag{10}$$

The conditional probability in (9) can be expressed as

$$P(\gamma_2 \leq x \,|\, \gamma_2 > \gamma_T) = \mathbf{1}_{(\gamma_T,\infty)}(x) \cdot \frac{F_{\gamma_2}(x) - F_{\gamma_2}(\gamma_T)}{1 - F_{\gamma_2}(\gamma_T)}, \tag{11}$$

where $\mathbf{1}_A(x)$ is the indicator function of A, which is equal to one when $x \in A$ and zero otherwise.

Introducing (10) in (8) and (11) in (9) yields

$$F_{\gamma_{\text{eff}}}(x) = F_{\gamma_1}(x) \cdot \min\left(1, \frac{F_{\gamma_2}(x)}{F_{\gamma_2}(\gamma_T)}\right) F_{\gamma_2}(\gamma_T) + \mathbf{1}_{(\gamma_T,\infty)}(x) \cdot \frac{F_{\gamma_2}(x) - F_{\gamma_2}(\gamma_T)}{1 - F_{\gamma_2}(\gamma_T)} \left[1 - F_{\gamma_2}(\gamma_T)\right], \tag{12}$$

which can be simplified to the more compact form

$$F_{\gamma_{\text{eff}}}(x) = F_{\gamma_1}(x) \cdot \min\left(F_{\gamma_2}(x), F_{\gamma_2}(\gamma_T)\right) + \mathbf{1}_{(\gamma_T,\infty)}(x) \cdot \left[F_{\gamma_2}(x) - F_{\gamma_2}(\gamma_T)\right]. \tag{13}$$

The expression in (13) can be rewritten as

$$F_{\gamma_{\text{eff}}}(x) = \begin{cases} F_{\gamma_1}(x)F_{\gamma_2}(x), & x \le \gamma_T, \quad (14a) \\ F_{\gamma_1}(x)F_{\gamma_2}(\gamma_T) + F_{\gamma_2}(x) - F_{\gamma_2}(\gamma_T), & \\ & x > \gamma_T. \quad (14b) \end{cases}$$

Introducing (2) and (4) in (14a) yields (7a). Similarly, introducing (2) and (4) in (14b) and simplifying yields (7b). □

Theorem 2 (CDF of SNR under MRC)**.** *The CDF of SNR for the proposed hybrid system under MRC is given by*

$$F_{\gamma_{\text{eff}}}(x) = \begin{cases} \frac{m^m}{\Gamma(m)} \sum_{j=0}^{\infty} \frac{K^j d_j}{j!(2\alpha\sigma^2)^{j+1}} \left[1 - \exp\left(-\frac{x}{\overline{\gamma}_1}\right)\right. & (15a) \\ \left. - \frac{2\sigma^2}{\overline{\gamma}_1} \sum_{k=0}^{j} \frac{(2\alpha\sigma^2)^k}{k!} \gamma\left(k+1, \frac{x}{2\sigma^2}\right)\right], x \le \gamma_T, & \\ \frac{m^m}{\Gamma(m)} \sum_{j=0}^{\infty} \frac{K^j d_j}{(j!)^2} \left[\gamma\left(j+1, \frac{x}{2\sigma^2}\right)\right. & (15b) \\ \left. - \exp\left(-\frac{x}{\overline{\gamma}_1}\right) \frac{\gamma(j+1, \alpha\gamma_T)}{(2\alpha\sigma^2)^{j+1}}\right], \quad x > \gamma_T, & \end{cases}$$

where $\alpha = (2\sigma^2)^{-1} - (\overline{\gamma}_1)^{-1}$.

Proof. When $\gamma_2 \le \gamma_T$ under MRC, $g(\gamma_1, \gamma_2) = \gamma_1 + \gamma_2$ and the PDF of γ_{eff} can be calculated as [40, eq. (6-45)]

$$f_{\gamma_{\text{eff}}}(x) = \int_0^x f_{\gamma_1}(x-y) f_{\gamma_2}(y) dy \tag{16}$$

$$= \frac{1}{\overline{\gamma}_1} \exp\left(-\frac{x}{\overline{\gamma}_1}\right) \frac{m^m}{\Gamma(m)} \sum_{j=0}^{\infty} \frac{K^j d_j}{(j!)^2} \frac{1}{(2\sigma^2)^{j+1}} \times \int_0^x y^j \exp\left(-y\left[\frac{1}{2\sigma^2} - \frac{1}{\overline{\gamma}_1}\right]\right) dy, \; x \le \gamma_T. \tag{17}$$

The integral in (17) can be solved with the assistance of [38, eq. (3.381.1)], which yields

$$f_{\gamma_{\text{eff}}}(x) = \frac{1}{\overline{\gamma}_1} \exp\left(-\frac{x}{\overline{\gamma}_1}\right) \frac{m^m}{\Gamma(m)} \sum_{j=0}^{\infty} \frac{K^j d_j}{(j!)^2} \frac{\gamma(j+1, \alpha x)}{(2\alpha\sigma^2)^{j+1}}, \quad x \le \gamma_T, \tag{18}$$

where $\alpha = (2\sigma^2)^{-1} - (\overline{\gamma}_1)^{-1}$. The solution in [38, eq. (3.381.1)] is valid for $\alpha > 0$, which implies $\overline{\gamma}_1 > \overline{\gamma}_2[(E_b/N_0)(1+K)]^{-1}$. This requirement is met in practice since $\overline{\gamma}_1 > \overline{\gamma}_2$ due to the higher path loss at higher frequencies (i.e., lower signal power) and larger bandwidths (i.e., higher noise power) in FR2.

The corresponding CDF when $\gamma_2 \le \gamma_T$, $F_{\gamma_{\text{eff}}}(x)$, can be calculated based on (18) as

$$F_{\gamma_{\text{eff}}}(x) = \int_0^x f_{\gamma_{\text{eff}}}(y) dy = \frac{1}{\overline{\gamma}_1} \frac{m^m}{\Gamma(m)} \sum_{j=0}^{\infty} \frac{K^j d_j}{(j!)^2} \frac{1}{(2\alpha\sigma^2)^{j+1}} \times \int_0^x \exp\left(-\frac{y}{\overline{\gamma}_1}\right) \gamma(j+1, \alpha y) dy, \; x \le \gamma_T. \tag{19}$$

By replacing the lower incomplete gamma function in (19) with its equivalent form in [38, eq. (8.352.1)] and solving the integral with the aid of [38, eq. (3.381.1)], (15a) is obtained.

When $\gamma_2 > \gamma_T$ under MRC, the CDF of the output SNR γ_{eff} can be expressed as

$$F_{\gamma_{\text{eff}}}(x) = G(x) + F_{\gamma_2}(x) - F_{\gamma_2}(\gamma_T), \qquad x > \gamma_T, \tag{20}$$

where $G(x)$ can be calculated as [40, eqs. (6-38) and (6-42)]

$$G(x) = \int_0^{\gamma_T} \int_0^{x-z} f_{\gamma_1}(y) f_{\gamma_2}(z) dy dz \tag{21}$$

$$= \int_0^{\gamma_T} f_{\gamma_2}(z) \left[\int_0^{x-z} f_{\gamma_1}(y) dy\right] dz \tag{22}$$

$$= \int_0^{\gamma_T} F_{\gamma_1}(x-z) f_{\gamma_2}(z) dz \tag{23}$$

$$= \int_0^{\gamma_T} f_{\gamma_2}(z) dz - \overline{\gamma}_1 \int_0^{\gamma_T} f_{\gamma_1}(x-z) f_{\gamma_2}(z) dz \tag{24}$$

$$= F_{\gamma_2}(\gamma_T) - \exp\left(-\frac{x}{\overline{\gamma}_1}\right) \frac{m^m}{\Gamma(m)} \times \sum_{j=0}^{\infty} \frac{K^j d_j}{(j!)^2} \frac{\gamma(j+1, \alpha\gamma_T)}{(2\alpha\sigma^2)^{j+1}}, \tag{25}$$

where the relation $F_{\gamma_1}(x-z) = 1 - \overline{\gamma}_1 f_{\gamma_1}(x-z)$ from (1)–(2) is introduced in (23) to obtain (24), which is then resolved using [38, eq. (3.381.1)]. Combining (4) and (25) with (20) and grouping terms yields (15b), which completes the proof. □

B. Probability Density Function of the SNR

Theorem 3 (PDF of SNR under SC)**.** *The PDF of SNR for the proposed hybrid system under SC is given by*

$$f_{\gamma_{\text{eff}}}(x) = \begin{cases} \frac{m^m}{\Gamma(m)} \sum_{j=0}^{\infty} \frac{K^j d_j}{(j!)^2} \left[\frac{1}{\overline{\gamma}_1} \exp\left(-\frac{x}{\overline{\gamma}_1}\right) \gamma\left(j+1, \frac{x}{2\sigma^2}\right)\right. & \\ \left. + \left(1 - \exp\left(-\frac{x}{\overline{\gamma}_1}\right)\right) \frac{1}{2\sigma^2} \exp\left(-\frac{x}{2\sigma^2}\right) \left(\frac{x}{2\sigma^2}\right)^j\right], & \\ \qquad x \le \gamma_T, \quad (26a) \\ \frac{m^m}{\Gamma(m)} \sum_{j=0}^{\infty} \frac{K^j d_j}{(j!)^2} \left[\frac{1}{2\sigma^2} \exp\left(-\frac{x}{2\sigma^2}\right) \left(\frac{x}{2\sigma^2}\right)^j\right. & \\ \left. + \frac{1}{\overline{\gamma}_1} \exp\left(-\frac{x}{\overline{\gamma}_1}\right) \gamma\left(j+1, \frac{\gamma_T}{2\sigma^2}\right)\right], & \\ \qquad x > \gamma_T. \quad (26b) \end{cases}$$

Proof. By differentiation of (7), using [38, eq. (8.356.4)]. □

Theorem 4 (PDF of SNR under MRC)**.** *The PDF of SNR for the proposed hybrid system under MRC is given by*

$$f_{\gamma_{\text{eff}}}(x)=\begin{cases}\dfrac{1}{\overline{\gamma}_1}\exp\left(-\dfrac{x}{\overline{\gamma}_1}\right)\dfrac{m^m}{\Gamma(m)}\displaystyle\sum_{j=0}^{\infty}\frac{K^j d_j}{(j!)^2}\frac{\gamma(j+1,\alpha x)}{(2\alpha\sigma^2)^{j+1}}, & x\le\gamma_T, \quad (27a)\\ \dfrac{m^m}{\Gamma(m)}\displaystyle\sum_{j=0}^{\infty}\frac{K^j d_j}{(j!)^2}\left[\frac{1}{2\sigma^2}\exp\left(-\frac{x}{2\sigma^2}\right)\left(\frac{x}{2\sigma^2}\right)^j\right. & \\ \left.+\dfrac{1}{\overline{\gamma}_1}\exp\left(-\dfrac{x}{\overline{\gamma}_1}\right)\frac{\gamma(j+1,\alpha\gamma_T)}{(2\alpha\sigma^2)^{j+1}}\right], & x>\gamma_T\ . \quad (27b)\end{cases}$$

Proof. By differentiation of (15), using [38, eq. (8.356.4)]. □

IV. Performance Analysis

A. Probabilities of Outage and Link Usage

In the context of URLLC, reliability is defined as the success probability of transmitting a specified amount of bytes within a certain delay target [4]. However, as discussed in Section I, the interest of this work lies explicitly in the reliability aspect of URLLC. When delay or latency are not explicitly included, other definitions of reliability can be considered [41], the most common one being the level of link connectivity guarantees, typically quantified in terms of the probability of outage [42]. As pointed out in [7], even when the latency is not explicitly quantified, the use of short packets and the reduction of the outage probability can enable URLLC. Therefore, the outage probability is also a suitable reliability metric for URLLC.

The probability that the proposed hybrid system is in outage is obtained as the probability that the instantaneous effective SNR at the receiver γ_{eff} falls below a given outage threshold γ_{out} that represents the minimum SNR required to ensure that a certain maximum BER is not exceeded. Such probability can be obtained as $P_{\text{out}} = P(\gamma_{\text{eff}} \le \gamma_{\text{out}}) = F_{\gamma_{\text{eff}}}(\gamma_{\text{out}})$, where $F_{\gamma_{\text{eff}}}(\cdot)$ is the CDF of the effective SNR at the receiver, which is given by (7) for SC and (15) for MRC.

In the proposed transmission scheme the mmWave (FR2) link is used with probability one (i.e., continuously). However, the sub-6 GHz (FR1) link is used only when the instantaneous channel quality in the FR2 link (in terms of the instantaneous SNR γ_2) falls below a certain threshold (γ_T). The probability that the FR1 link is in use is given by $P_{\text{FR1}} = P(\gamma_2 \le \gamma_T) = F_{\gamma_2}(\gamma_T)$, where $F_{\gamma_2}(\cdot)$ is given by (4). A high P_{FR1} implies that the FR1 link needs to be used often as a backup for the FR2 link, while a low P_{FR1} means that the FR1 link is more often available for other data transmissions.

Note that when $\gamma_T = \gamma_{\text{out}}$ the probability of using the FR1 link coincides with the outage probability of the FR2 link.

B. Average Bit Error Rate

The Average Bit Error Rate (ABER) over a fading channel, denoted by $\overline{P}_b$, can be obtained as [34, eq. (8.102)]

$$\overline{P}_b = \int_0^\infty P_b(x) f_\gamma(x) dx, \quad (28)$$

where $P_b(\gamma)$ represents the conditional bit-error probability for a given SNR γ and $f_\gamma(\cdot)$ is the PDF of the instantaneous SNR per symbol. Without loss of generality, the analysis presented in this section will consider binary modulations, for which the following general expression can be used [43, eq. (13)]

$$P_b(\gamma) = \frac{\Gamma(b, a\gamma)}{2\Gamma(b)}, \quad (29)$$

where $\Gamma(\cdot,\cdot)$ represents the upper incomplete gamma function [38, eq. (8.350.2)] and $a, b \in \{\frac{1}{2}, 1\}$ are modulation-specific parameters (see [34, Table 8.1] for details).

Introducing (29) in (28), integrating by parts [38, 2.02.5] and using [38, 8.356.4], the ABER can be rewritten in the following more convenient form

$$\overline{P}_b = \frac{a^b}{2\Gamma(b)} \int_0^\infty e^{-ax} x^{b-1} F_\gamma(x) dx, \quad (30)$$

The solution to the integral in (30) for the Rayleigh channel can be obtained with the aid of [38, eq. (3.381.4)], which yields $\overline{P}_b = \frac{1}{2}[1 - (1 + 1/a\overline{\gamma}_1)^{-b}]$. The solution for the FTR channel is provided in [37, eq. (16)] together with [39, eq. (16)]. For the proposed hybrid scheme, (30) is calculated as

$$\overline{P}_b = \frac{a^b}{2\Gamma(b)} \int_0^{\gamma_T} e^{-ax} x^{b-1} F_{\gamma_{\text{eff}}}(x) dx \quad (31)$$

$$+ \frac{a^b}{2\Gamma(b)} \int_{\gamma_T}^\infty e^{-ax} x^{b-1} F_{\gamma_{\text{eff}}}(x) dx, \quad (32)$$

where the expression for $F_{\gamma_{\text{eff}}}(x)$ in each integral is according to the corresponding SNR interval. The result in (31)–(32) can be used to derive expressions for the ABER of the proposed hybrid transmission scheme under SC and MRC.

Theorem 5 (ABER under SC)**.** *The ABER of the proposed hybrid system under SC is given by*

$$\overline{P}_b = \frac{a^b}{2\Gamma(b)} \frac{m^m}{\Gamma(m)} \sum_{j=0}^{\infty} \frac{K^j d_j}{(j!)^2} \left(P_A - P_B - P_C\right), \quad (33)$$

where:

$$P_A = \frac{\Gamma(b+j+1)(2\sigma^2)^b}{(j+1)(1+2a\sigma^2)^{b+j+1}} \times {}_2F_1\left(1, b+j+1; j+2; \frac{1}{1+2a\sigma^2}\right), \quad (34)$$

$$P_B = j!\left[\left(a+\frac{1}{\overline{\gamma}_1}\right)^{-b}\gamma\left(b, \left[a+\frac{1}{\overline{\gamma}_1}\right]\gamma_T\right) - \sum_{k=0}^{j}\frac{(a+\beta)^{-(k+b)}\,\gamma\left(k+b, [a+\beta]\,\gamma_T\right)}{k!(2\sigma^2)^k}\right], \quad (35)$$

$$P_C = \left(a+\frac{1}{\overline{\gamma}_1}\right)^{-b}\Gamma\left(b, \left[a+\frac{1}{\overline{\gamma}_1}\right]\gamma_T\right)\gamma\left(j+1, \frac{\gamma_T}{2\sigma^2}\right), \quad (36)$$

with ${}_2F_1(\cdot,\cdot;\cdot;\cdot)$ denoting the Gauss hypergeometric function [38, eq. (9.100)] and $\beta = (2\sigma^2)^{-1} + (\overline{\gamma}_1)^{-1}$.

Proof. Introducing (7a) in (31) and (7b) in (32), and expanding all the terms, an expression of the form (33) is obtained with

$$P_A = \int_0^{\infty} \exp(-ax)\, x^{b-1} \gamma\left(j+1, \frac{x}{2\sigma^2}\right) dx, \tag{37}$$

$$P_B = \int_0^{\gamma_T} \exp\left(-\left[a+\frac{1}{\overline{\gamma}_1}\right]x\right) x^{b-1} \gamma\left(j+1, \frac{x}{2\sigma^2}\right) dx, \tag{38}$$

$$P_C = \gamma\left(j+1, \frac{\gamma_T}{2\sigma^2}\right) \int_{\gamma_T}^{\infty} \exp\left(-\left[a+\frac{1}{\overline{\gamma}_1}\right]x\right) x^{b-1} dx. \tag{39}$$

The integral in (37) is resolved by using [38, eq. (6.455.2)], which yields (34). The integral in (38) is solved by introducing [38, eq. (8.352.1)] and then employing [38, eq. (3.381.1)], which yields (35). The integral in (39) is resolved with the help of [38, eq. 3.381.3], which yields (36). □

Theorem 6 (ABER under MRC)**.** *The ABER of the proposed hybrid system under MRC is given by*

$$\overline{P}_b = \frac{a^b}{2\Gamma(b)} \frac{m^m}{\Gamma(m)} \sum_{j=0}^{\infty} \frac{K^j d_j}{j!} \left(\frac{P_D - P_E - P_F}{(2\alpha\sigma^2)^{j+1}} + \frac{P_G - P_H}{j!} \right), \tag{40}$$

where

$$P_D = a^{-b}\gamma(b, a\gamma_T), \tag{41}$$

$$P_E = \left(a+\frac{1}{\overline{\gamma}_1}\right)^{-b} \gamma\left(b, \left[a+\frac{1}{\overline{\gamma}_1}\right]\gamma_T\right), \tag{42}$$

$$P_F = \frac{2\sigma^2}{\overline{\gamma}_1} \sum_{k=0}^{j} (2\alpha\sigma^2)^k \left[a^{-b}\gamma(b, a\gamma_T) - \sum_{l=0}^{k} \frac{\left(a+\frac{1}{2\sigma^2}\right)^{-(l+b)} \gamma\left(l+b, \left[a+\frac{1}{2\sigma^2}\right]\gamma_T\right)}{l!(2\sigma^2)^l} \right], \tag{43}$$

$$P_G = (j!) \left[a^{-b}\Gamma(b, a\gamma_T) - \sum_{k=0}^{j} \frac{\left(a+\frac{1}{2\sigma^2}\right)^{-(k+b)} \Gamma\left(k+b, \left[a+\frac{1}{2\sigma^2}\right]\gamma_T\right)}{k!(2\sigma^2)^k} \right], \tag{44}$$

$$P_H = \frac{\gamma(j+1, \alpha\gamma_T)}{(2\alpha\sigma^2)^{j+1}} \left(a+\frac{1}{\overline{\gamma}_1}\right)^{-b} \Gamma\left(b, \left[a+\frac{1}{\overline{\gamma}_1}\right]\gamma_T\right), \tag{45}$$

with $\alpha = (2\sigma^2)^{-1} - (\overline{\gamma}_1)^{-1}$.

Proof. Introducing (15a) in (31) and (15b) in (32), and expanding terms, an expression of the form (40) is obtained with

$$P_D = \int_0^{\gamma_T} \exp(-ax)\, x^{b-1} dx, \tag{46}$$

$$P_E = \int_0^{\gamma_T} \exp\left(-\left[a+\frac{1}{\overline{\gamma}_1}\right]x\right) x^{b-1} dx, \tag{47}$$

$$P_F = \frac{2\sigma^2}{\overline{\gamma}_1} \sum_{k=0}^{j} \frac{(2\alpha\sigma^2)^k}{k!} \times \int_0^{\gamma_T} \exp(-ax)\, x^{b-1} \gamma\left(k+1, \frac{x}{2\sigma^2}\right) dx, \tag{48}$$

$$P_G = \int_{\gamma_T}^{\infty} \exp(-ax)\, x^{b-1} \gamma\left(j+1, \frac{x}{2\sigma^2}\right) dx, \tag{49}$$

$$P_H = \frac{\gamma(j+1, \alpha\gamma_T)}{(2\alpha\sigma^2)^{j+1}} \int_{\gamma_T}^{\infty} \exp\left(-\left[a+\frac{1}{\overline{\gamma}_1}\right]x\right) x^{b-1} dx. \tag{50}$$

The integrals in (46) and (47) can both be resolved by using [38, eq. (3.381.1)], which yields (41) and (42), respectively. The integral in (48) is solved by introducing [38, eq. (8.352.1)] and then making use of [38, eq. (3.381.1)], which yields (43). Similarly, the integral in (49) is resolved by first introducing [38, eq. (8.352.1)] and then employing [38, eq. (3.381.3)], which yields (44). Finally, the integral in (50) can be resolved with the assistance of [38, eq. 3.381.3], which yields (45). □

C. Ergodic Capacity

The ergodic capacity C (in bit/s) of a fading channel with bandwidth B (in Hz) for a constant-power transmitter with optimum rate adaptation is given by [34, eq. (15.21)]

$$\begin{aligned} C &= B \int_0^{\infty} \log_2(1+x) f_\gamma(x) dx \\ &= \frac{B}{\ln 2} \int_0^{\infty} \ln(1+x) f_\gamma(x) dx, \end{aligned} \tag{51}$$

where $f_\gamma(\cdot)$ is the PDF of the instantaneous SNR per symbol. Solutions to the integral in (51) for the Rayleigh and FTR channels are provided in [34, eq. (15.26)] and [37, eq. (12)], respectively. For the proposed scheme, (51) is calculated as

$$C = \frac{B_1}{\ln 2} \int_0^{\gamma_T} \ln(1+x) f_{\gamma_{\text{eff}}}(x) dx \tag{52}$$

$$+ \frac{B_2}{\ln 2} \int_{\gamma_T}^{\infty} \ln(1+x) f_{\gamma_{\text{eff}}}(x) dx, \tag{53}$$

where B_1 and B_2 are the bandwidths of the FR1 and FR2 links, respectively, and the expression for $f_{\gamma_{\text{eff}}}(x)$ in each integral is according to the corresponding SNR interval. Note that when γ_2 falls below γ_T and the FR1 link is activated, the same bit stream needs to be transmitted in both links (FR1 and FR2) in order to combine them with a diversity technique (SC or MRC) at the receiver. Because the bit stream in both links needs to be identical and the available bandwidth is typically lower in the FR1 link than in the FR2 link[1] (i.e., $B_1 < B_2$), the transmitter needs to reduce the bit rate (by

[1]If $B_1 \geq B_2$ then mobile operators would have little incentive to use FR2 bands given their poorer propagation characteristics, which combined with a lower bandwidth would provide a much lower capacity than FR1 bands.

adapting modulation and coding schemes) when the FR1 link is activated. Even though the FR2 link has a higher channel bandwidth, when the FR1 link is activated the bit stream transmitted through the FR2 link only requires a bandwidth B_1, so effectively a bandwidth B_1 is actually used in both links (to transmit the same bit stream) when the FR1 link is activated[2]. Therefore, from the point of view of the ergodic capacity (i.e., maximum amount of bits that can be transmitted per unit time) a bandwidth B_1 needs to be considered in (52).

This section derives expressions for the ergodic capacity of the proposed hybrid transmission scheme under SC and MRC.

Theorem 7 (Ergodic capacity under SC)**.** *The ergodic capacity of the proposed hybrid system under SC is given by*

$$C = \frac{1}{\ln 2}\frac{m^m}{\Gamma(m)}\sum_{j=0}^{\infty}\frac{K^j d_j}{j!} \times \big[B_1(\eta_A - \eta_B + \eta_C - \eta_D) + B_2(\eta_E + \eta_F)\big], \tag{54}$$

where η_A, η_B, η_C, η_D, η_E, η_F are given by (56)–(61) at the bottom of the next page, $E_1(x) = \int_x^\infty e^{-t}t^{-1}\,dt = \int_1^\infty e^{-xt}t^{-1}\,dt$ is the exponential integral function of first order [38, eq. (3.351.5)] and $\beta = (2\sigma^2)^{-1} + (\overline{\gamma}_1)^{-1}$.

Proof. Introducing (26a) in (52) and (26b) in (53), replacing the lower incomplete gamma function with its equivalent form in [38, eq. (8.352.1)] and expanding all the terms, integrals of the form $I(s,t) = \int_s^t \ln(1+x)x^p e^{-qx}dx$ are obtained. The solution to $I(0,\infty)$ is given by [44, eq. (A.3)] and the solution to $I(\gamma_T,\infty)$ is given by [44, eq. (A.2)], while $I(0,\gamma_T) = I(0,\infty) - I(\gamma_T,\infty)$. Substituting the equalities $\Gamma(0,x) = E_1(x)$ and $\Gamma(1,x) = e^{-x}$ in the obtained results and grouping terms, (54) is obtained. Even though the procedure is tedious, it involves standard mathematical manipulations. □

Theorem 8 (Ergodic capacity under MRC)**.** *The ergodic capacity of the proposed hybrid system under MRC is given by*

$$C = \frac{1}{\ln 2}\frac{m^m}{\Gamma(m)}\sum_{j=0}^{\infty}\frac{K^j d_j}{j!}\frac{1}{(2\alpha\sigma^2)^{j+1}} \times \big[B_1(\eta_A - \eta_G) + B_2\big((2\alpha\sigma^2)^{j+1}\eta_E + \eta_H\big)\big], \tag{55}$$

where η_G and η_H are given by (62) and (63) at the bottom of the page, respectively, $E_1(x) = \int_x^\infty e^{-t}t^{-1}\,dt = \int_1^\infty e^{-xt}t^{-1}\,dt$ is the exponential integral function of first order [38, eq. (3.351.5)] and $\alpha = (2\sigma^2)^{-1} - (\overline{\gamma}_1)^{-1}$.

Proof. See proof of Theorem 7, using (27) instead of (26). □

V. Results

A. Evaluation Scenario

The performance of the proposed hybrid transmission technique is evaluated considering band n78 in FR1, which has a central frequency $f_1 = 3.55$ GHz [28, Table 5.2-1], and band n257 in FR2, which has a central frequency $f_2 = 28$ GHz [29, Table 5.2-1]. The User Equipment (UE) channel bandwidth is assumed to be $B_1 = 20$ MHz in the FR1 link [28, Table 5.3.5-1] and $B_2 = 50$ MHz in the FR2 link [29, Table 5.3.5-1].

Rayleigh and FTR ($m = 20$, $K = 5$, $\Delta = 0.1$) fading models are assumed for the FR1 and FR2 bands, respectively. Notice that the average SNR in the FR1 link will be higher than in the FR2 link due to the lower path loss associated with lower propagation frequencies, however both SNR values are not independent since both links are subject to the same physical propagation distance. To ensure realistic pairs of SNR values, the received power in both bands is calculated as $P_R = P_T\,G_T\,G_R\,[c/(4\pi f)]^2\,d^{-\delta}$, where $P_T = 10$ dBm is the transmitted power, $G_T = 40$ dBi and $G_R = 40$ dBi are the gains of the transmitter and receiver antennas, respectively, $c = 3{\cdot}10^8$ m/s is the speed of light, f is the central frequency of each band (f_1 or f_2), $d = 100$ m is the physical distance between the transmitter and receiver antennas, and $\delta = 3.4$ is the path loss exponent (which is an appropriate value for non-line-of-sight conditions both in sub-6 GHz and mmWave bands [35], [45], [46]). The average SNR of each band ($\overline{\gamma}_1$ or $\overline{\gamma}_2$) is obtained as $\overline{\gamma} = P_R/P_N$, with the receiver's noise power calculated as $P_N = k_B T_0 B F$, where $k_B = 1.38{\cdot}10^{-23}$ J·K^{-1} is the Boltzmann constant, $T_0 = 290$ K is the reference room temperature, B is the bandwidth of the link in each band (B_1 or B_2) and F represents the receiver's noise factor (equivalent to a noise figure of 4 dB). The selected parameters lead to an equivalent noise floor of -110 dBm/MHz.

For evaluation purposes, the general BER model of (29) is particularised to $a = b = 1$, which corresponds to a differentially-encoded coherent BPSK modulation [34, Table 8.1]. The switching threshold γ_T is set assuming that the maximum tolerable BER for a successful demodulation of the received signal is 10^{-9} (higher values such as 10^{-6} were also evaluated but this was not observed to have a significant impact).

Unless otherwise stated, the parameter values presented in this subsection will be employed by default in this study.

B. Validation of the SNR Statistics

Fig. 2 compares the analytic results presented in Section III with their Monte Carlo simulation counterparts. Notice that results are plotted in logarithmic axes for a better detail of appreciation in the low SNR regime (around the switching threshold). For the proposed hybrid transmission scheme, the switching threshold is set to $\gamma_T = \gamma_{\text{out}}$, where γ_{out} can be obtained from (29). For a target BER of 10^{-9} and $a = b = 1$ the obtained switching threshold is $\gamma_T = 13$ dB. As it can be appreciated, for SNR values above γ_T the effective SNR follows the PDF for the FR2 link while for SNR values below γ_T it follows the PDF of the dual transmission scheme (according to the considered diversity technique). In all cases, analytic and simulation results match perfectly, thus corroborating the correctness of the results presented in Section III.

Subsequent results presented later on will be validated in their respective figures either with Monte Carlo simulations (when they relate to the SNR distribution, such as the probabilities of outage and link usage) or by numeric integration (when they relate to the ABER or ergodic capacity).

[2]In this case, the unused bandwidth in the FR2 link could potentially be utilised for other data transmissions and/or to introduce additional redundancy in the transmitted signal in order to improve the signal decodability (this would require novel diversity techniques specifically designed to this end, which is beyond the scope of this study and is suggested as future work).

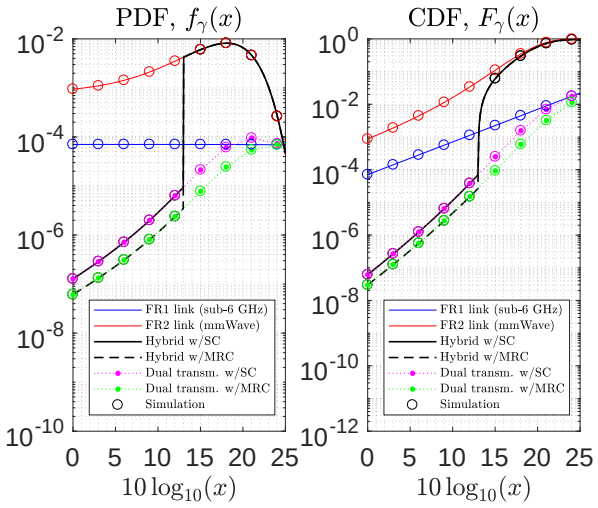

Fig. 2: Validation of the SNR statistics ($d = 1000$ m).

C. Performance Evaluation

The performance of the proposed hybrid scheme is evaluated based on the analytic results presented in Section IV. The performance is compared with the two limiting cases obtained for $\gamma_T = 0$ (single link transmission scenario where only the FR2 link is used) and $\gamma_T \to \infty$ (dual link transmission scenario where the system transmits continuously in both FR1 and FR2 links). These two cases provide appropriate baseline scenarios for a fair performance evaluation of the proposed hybrid transmission scheme. The performance of transmitting over the FR1 link alone is included for comparison purposes as well. It is worth mentioning that, from a performance point of view, operation in the high SNR regime ($\overline{\gamma}_2 \to \infty$) is equivalent to $\gamma_T = 0$ while operation in the low SNR regime ($\overline{\gamma}_2 \to 0$) is equivalent to $\gamma_T \to \infty$, respectively.

Fig. 3 shows the probability of outage as a function of the maximum tolerable BER for a differentially-encoded coherent BPSK modulation ($a = b = 1$, [34, Table 8.1]). When the system tolerates a higher BER the associated outage threshold γ_{out}, which can be obtained by solving (29) for γ, decreases and so does the probability of outage P_{out}. The highest P_{out} is obtained for the FR2 link alone given its more challenging propagation conditions (i.e., higher path loss and lower average SNR). Transmitting over the FR1 link alone would decrease P_{out}, however the best outage performance is obtained when both links, FR1 and FR2, are used continuously in the dual transmission scenario. The proposed hybrid transmission scheme can achieve that same level of best performance as long as the switching threshold γ_T is greater than the outage threshold ($\gamma_T \geq \gamma_{\text{out}}$) since this allows the activation of the FR1 link before the FR2 link falls in outage; if such condition is met, the proposed hybrid system can only fall in outage when transmitting over both links (i.e., the most reliable transmission approach) falls in outage as well. Under such scenario, MRC provides a lower outage probability than SC, as expected. On the other hand, if $\gamma_T < \gamma_{\text{out}}$ the FR2 link may temporarily fall in outage before the FR1 link is activated and, even though this still results in a better outage performance than transmission over the FR2 link alone, the outage performance will be worse than when $\gamma_T \geq \gamma_{\text{out}}$ (worse than in the FR1 link alone as well). In this case, the lower the switching threshold γ_T, the higher the

$$\eta_A = \exp\left(\frac{1}{\overline{\gamma}_1}\right)\left[E_1\left(\frac{1}{\overline{\gamma}_1}\right) - E_1\left(\frac{1+\gamma_T}{\overline{\gamma}_1}\right)\right] - \ln(1+\gamma_T)\exp\left(-\frac{\gamma_T}{\overline{\gamma}_1}\right) \tag{56}$$

$$\eta_B = \frac{1}{\beta\overline{\gamma}_1}\sum_{k=0}^{j}\frac{1}{(2\beta\sigma^2)^k}\left[\sum_{l=0}^{k}\left\{\beta^{k-l}e^{\beta}\Gamma(-k+l,\beta) - \frac{\Gamma(l,\beta(1+\gamma_T))}{\Gamma(l+1)}\frac{\Gamma(k-l+1,-\beta)}{\Gamma(k-l+1)}\right\} - \ln(1+\gamma_T)\frac{\Gamma(k+1,\beta\gamma_T)}{\Gamma(k+1)}\right] \tag{57}$$

$$\eta_C = \sum_{l=0}^{j}\left\{\frac{\exp(1/2\sigma^2)}{(2\sigma^2)^{j-l}}\Gamma\left(-j+l,\frac{1}{2\sigma^2}\right) - \frac{\Gamma\left(l,\frac{1+\gamma_T}{2\sigma^2}\right)}{\Gamma(l+1)}\frac{\Gamma\left(j-l+1,-\frac{1}{2\sigma^2}\right)}{\Gamma(j-l+1)}\right\} - \ln(1+\gamma_T)\frac{\Gamma\left(j+1,\frac{\gamma_T}{2\sigma^2}\right)}{\Gamma(j+1)} \tag{58}$$

$$\eta_D = \frac{1}{(2\beta\sigma^2)^{j+l}}\left[\sum_{l=0}^{j}\left\{\beta^{j-l}e^{\beta}\Gamma(-j+l,\beta) - \frac{\Gamma(l,\beta(1+\gamma_T))}{\Gamma(l+1)}\frac{\Gamma(j-l+1,-\beta)}{\Gamma(j-l+1)}\right\} - \ln(1+\gamma_T)\frac{\Gamma(j+1,\beta\gamma_T)}{\Gamma(j+1)}\right] \tag{59}$$

$$\eta_E = \sum_{l=0}^{j}\frac{\Gamma\left(l,\frac{1+\gamma_T}{2\sigma^2}\right)}{\Gamma(l+1)}\frac{\Gamma\left(j-l+1,-\frac{1}{2\sigma^2}\right)}{\Gamma(j-l+1)} + \ln(1+\gamma_T)\frac{\Gamma\left(j+1,\frac{\gamma_T}{2\sigma^2}\right)}{\Gamma(j+1)} \tag{60}$$

$$\eta_F = \frac{\gamma\left(j+1,\frac{\gamma_T}{2\sigma^2}\right)}{\Gamma(j+1)}\left[\exp\left(\frac{1}{\overline{\gamma}_1}\right)E_1\left(\frac{1+\gamma_T}{\overline{\gamma}_1}\right) + \ln(1+\gamma_T)\exp\left(-\frac{\gamma_T}{\overline{\gamma}_1}\right)\right] \tag{61}$$

$$\eta_G = \frac{2\sigma^2}{\overline{\gamma}_1}\sum_{k=0}^{j}(2\alpha\sigma^2)^k\left[\sum_{l=0}^{k}\left\{\frac{\exp(1/2\sigma^2)}{(2\sigma^2)^{k-l}}\Gamma\left(-k+l,\frac{1}{2\sigma^2}\right) - \frac{\Gamma\left(l,\frac{1+\gamma_T}{2\sigma^2}\right)}{\Gamma(l+1)}\frac{\Gamma\left(k-l+1,-\frac{1}{2\sigma^2}\right)}{\Gamma(k-l+1)}\right\} - \ln(1+\gamma_T)\frac{\Gamma\left(k+1,\frac{\gamma_T}{2\sigma^2}\right)}{\Gamma(k+1)}\right] \tag{62}$$

$$\eta_H = \frac{\gamma\left(j+1,\alpha\gamma_T\right)}{\Gamma(j+1)}\left[\exp\left(\frac{1}{\overline{\gamma}_1}\right)E_1\left(\frac{1+\gamma_T}{\overline{\gamma}_1}\right) + \ln(1+\gamma_T)\exp\left(-\frac{\gamma_T}{\overline{\gamma}_1}\right)\right] \tag{63}$$

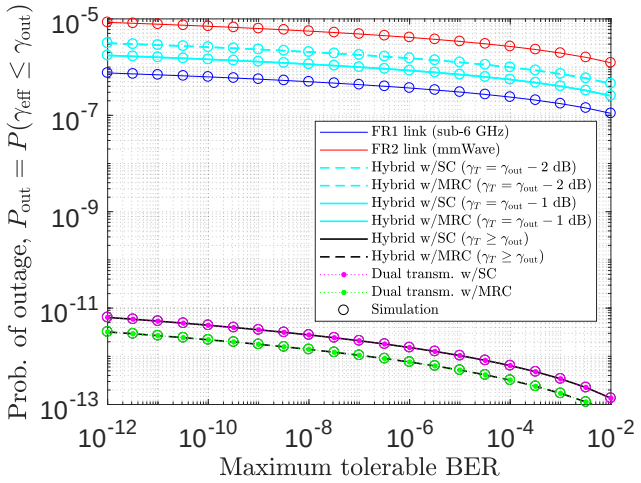

Fig. 3: Outage probability versus maximum tolerable BER.

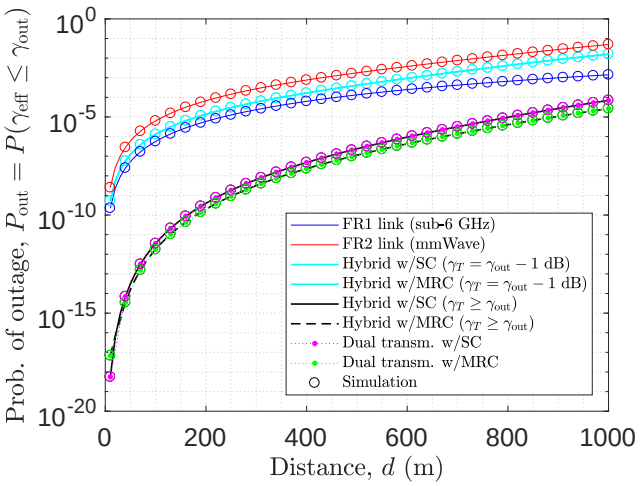

Fig. 4: Outage probability versus communication distance.

outage probability (regardless of which diversity technique is used). Therefore, by properly selecting the switching threshold ($\gamma_T \geq \gamma_{\text{out}}$), the proposed hybrid scheme can deliver the same level of link reliability as continuously transmitting over both links, however using the FR1 link only when it is really needed (and leaving it available for other transmissions otherwise). The discussion above indicates that a suitable choice for the switching threshold from the point of view of the reliability performance is any value that meets the condition $\gamma_T \geq \gamma_{\text{out}}$. Selecting lower values of γ_T results in a degradation of the reliability performance. On the other hand, selecting values of γ_T greater than γ_{out} ensures that the proposed hybrid scheme delivers the best reliability that can be attained. It is worth noting that increasing γ_T above γ_{out} does not improve the reliability performance any further, however affects the extent to which the FR1 link is used (as discussed later on).

Fig. 4 illustrates the outage performance as a function of the distance between transmitter and receiver. As it can be observed, for a reliability requirement of $P_{\text{out}} = 10^{-5}$ the FR2 link can provide a maximum communication distance of about 100 m. The proposed hybrid transmission scheme and the dual transmission scheme can both extend the communication distance to about 800 m with SC diversity and 900 m with MRC diversity. However, as shown in Fig. 5, at those distances the proposed hybrid transmission scheme only needs to use the FR1 link around 2% and 4% of the time, respectively (for $\gamma_T = \gamma_{\text{out}} + 1$ dB), meaning that most of the time the FR1 link would remain available for other data transmissions (it would be required to backup the FR2 link only very occasionally). Thus, by only reducing the FR1 link availability by 2%–4%, the proposed hybrid transmission scheme can provide an 8/9-fold increase in the FR2 link communication range. Compared to the dual transmission scheme, which would use the FR1 link 100% of the time as a dedicated (non-shared) resource, the proposed hybrid scheme can improve the link reliability with a dramatically higher level of resource efficiency.

It is worth noting that increasing the switching threshold γ_T above γ_{out} does not further reduce the outage probability (Fig. 4) but increases the FR1 link usage (Fig. 5). Therefore,

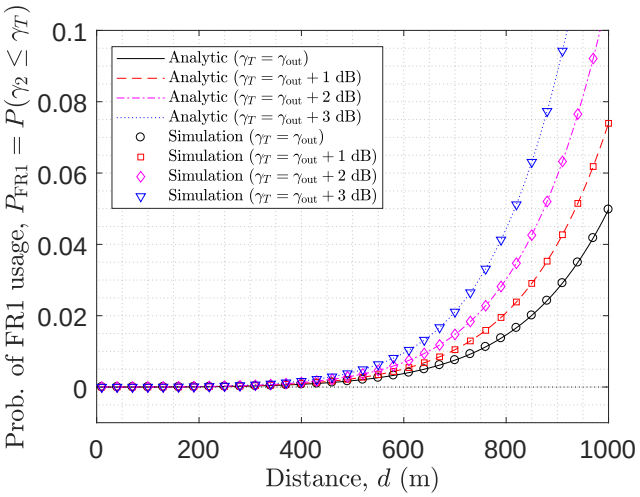

Fig. 5: FR1 link usage probability versus communication distance.

taking into account that the switching threshold γ_T should meet the condition $\gamma_T \geq \gamma_{\text{out}}$ in order to obtain the highest attainable reliability as discussed earlier, it becomes evident that the choice $\gamma_T = \gamma_{\text{out}}$ provides the optimum trade-off between overall system reliability and usage efficiency of radio resources. However, in a practical implementation this choice could potentially lead to momentary outages due to electronic circuit switching delays, which could severely degrade the outage performance as shown in Fig. 4 ($\gamma_T < \gamma_{\text{out}}$). Thus, some safety margin should be allowed (e.g., $\gamma_T = \gamma_{\text{out}} + 1$ dB), at the expense of slightly sacrificing some FR1 link availability, to ensure that the FR1 link is activated when needed.

The ABER performance, which is illustrated in Fig. 6, follows in general a very similar pattern as the outage probability shown in Fig. 4, hence similar comments are applicable. The most remarkable difference is that the ABER is not degraded as severely as the outage probability when $\gamma_T < \gamma_{\text{out}}$. This can be explained by the fact that $\overline{P}_b$ is an average of probabilities while P_{out} represents the probability that a particular event (outage) occurs. Hence, a slight reduction of the switching threshold γ_T below the outage threshold γ_{out} leads to a

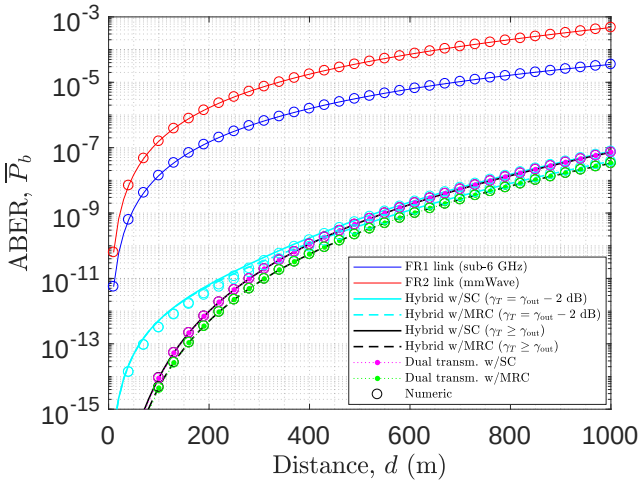

Fig. 6: ABER versus communication distance.

significant increase in the occurrence of outages but only a slight increase in the rate of bit-errors at the receiver.

The performance in terms of the ergodic capacity is shown in Fig. 7. Similar to the ABER, the capacity is not significantly affected by small variations of the switching threshold γ_T above or below the outage threshold γ_{out}, hence results are shown only for the case $\gamma_T = \gamma_{\text{out}}$ for the benefit of clarity. Three different configurations of the transmitter and receiver antenna gains are considered in order to emulate the effect of various link budgets. Notice that in all cases the capacity of the dual-link transmission scheme (with both SC and MRC diversity) is very similar to the capacity of the FR1 link alone (indistinguishable in Fig. 7). The explanation for this is that when the system transmits simultaneously in both links (FR1 and FR2), the bit-streams over both links need to be identical in order to combine them at the receiver with a diversity technique (SC or MRC). Since the FR1 link has a lower bandwidth than the FR2 link, the transmitter needs to reduce the bit-rate so that the generated bit-stream can fit within the bandwidth B_1 available in the FR1 link. As a result, the bit-rate of the transmitted signal is constrained by the bandwidth B_1. Therefore, from the point of view of the ergodic capacity, the effective bandwidth used for data transmission by the dual-link scheme is B_1, the same as in the FR1 link alone, hence the resulting capacity is very similar. As a matter of fact, when the dual-link transmission scheme is employed, the MRC capacity is actually slightly higher than the SC capacity, and both are slightly higher than the capacity provided by the FR1 link alone, which is due to the SNR gain obtained from diversity. However, the difference is negligible when compared to the other cases, thus the same line type (solid blue line) is used to represent the FR1 link and the dual-link transmission scheme (with both SC and MRC diversity) for the benefit of clarity.

Under favourable link budget (Fig. 7a), the SNR experienced in the FR2 link is good enough to prescind from the FR1 link and, as a result, the proposed hybrid transmission scheme transmits in the FR2 link most of the time (as observed at the bottom of Fig. 7a). This leads to a channel capacity very similar to that offered by the FR2 link alone, which is higher than the capacity provided by the FR1 link (and the dual transmission scheme) for all the considered distances due to the larger amount of bandwidth available in the FR2 link ($B_2 = 2.5B_1$). When the link budget degrades (Figs. 7b and 7c), the experienced channel quality in the FR2 link degrades as well and consequently the proposed hybrid scheme needs to rely more often on the FR1 link as a backup, which can be noticed from the higher FR1 link usage probability (P_{FR1}). As discussed above, when the FR1 link is activated the transmitter needs to reduce the bit-rate so the generated signal can fit within the bandwidth B_1 available in the FR1 link. However, as counterintuitive as it may seem, this does not result in a reduction of the channel capacity for the proposed hybrid scheme, which indeed increases when the FR1 link is activated as appreciated in Figs. 7b and 7c. Notice that in these two cases the probability of using the FR1 link increases as the FR1 link begins to provide a higher capacity than the FR2 link. Even though the available bandwidth is significantly lower in the FR1 link than in the FR2 link, the FR1 link can provide a higher capacity if the experienced SNR is sufficiently large to compensate the lower amount of bandwidth available (i.e., much higher spectral efficiency). Activating the FR1 link in such cases can significantly increase the resulting capacity, even though the effective transmission bandwidth is lower (but the effective channel quality is comparatively much better). Notice that the capacity of the proposed hybrid system is also noticeably higher than that attained by the dual transmission scheme. This is because the dual link scheme transmits continuously in both links (FR1 and FR2) and therefore is constrained to always do so according to a bandwidth B_1 regardless of the instantaneous channel quality, while the proposed hybrid scheme can benefit from a much higher transmission bandwidth B_2 when the channel quality is good enough, which ends up delivering a much higher capacity. Only when the channel quality is severely degraded due to a very unfavourable link budget (e.g., low antenna gain and long communication distance as in Fig. 7c) the capacity of the proposed scheme falls to match that of the dual transmission scheme, which is still higher than that of the FR2 link alone.

Some interesting insights can be gained from a careful observation of Fig. 7c. Notice that for more favourable link budgets (which in Fig. 7c can be associated to short communication distances) the proposed hybrid scheme transmits most of the time using the FR2 link only, which allows the system to benefit from the larger bandwidth available in this band in order to achieve a higher channel capacity. On the other hand, for less favourable link budgets (which in Fig. 7c can be associated to long communication distances) the proposed hybrid scheme relies on the FR1 link as a backup in order to overcome the degraded channel quality conditions in the FR2 link, which leads to a higher capacity than transmitting in the FR2 link only. For intermediate distances between these two extremes, the proposed hybrid scheme adjusts the FR1 link usage probability proportionally to the experienced channel quality. The dynamic adaptation offered by the hybrid scheme achieves the highest attainable capacity (out of all the considered transmission options/schemes) in all cases.

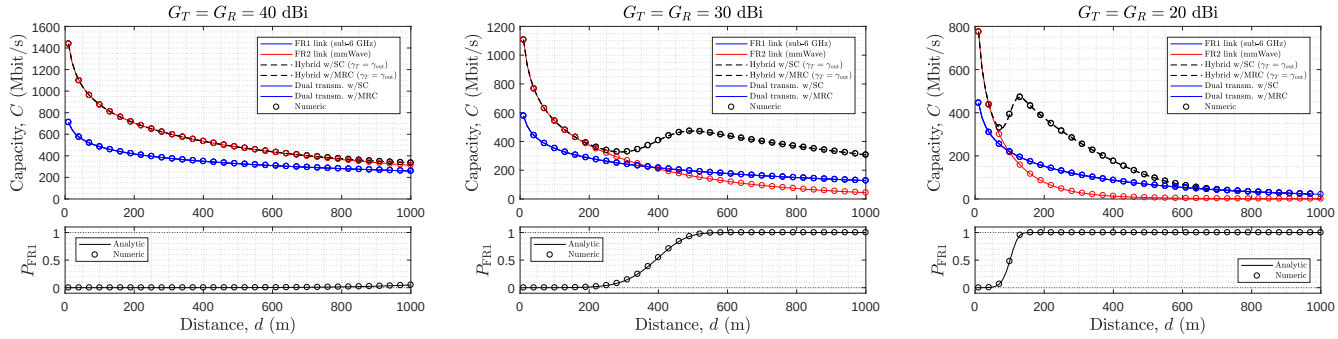

(a) (b) (c)

Fig. 7: Ergodic capacity (top) and FR1 link usage probability (bottom) versus communication distance for various transmitter and receiver antenna gains: (a) $G_T = G_R = 40$ dBi, (b) $G_T = G_R = 30$ dBi, and (c) $G_T = G_R = 20$ dBi.

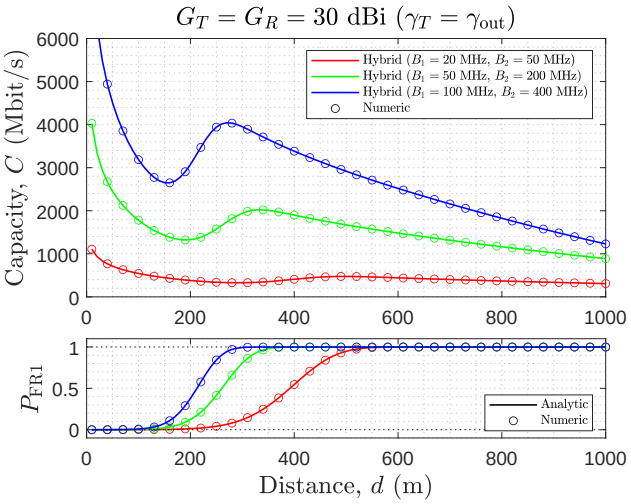

Fig. 8: Ergodic capacity (top) and FR1 link usage probability (bottom) versus communication distance for various bandwidth configurations with $G_T = G_R = 30$ dBi and $\gamma_T = \gamma_{\text{out}}$.

Therefore, it can be concluded that the overall link capacity is positively affected by the application of the proposed scheme.

For a more complete evaluation, Fig. 8 shows the ergodic capacity of the proposed hybrid transmission scheme for various bandwidth configurations. The figure shows the capacity not only for $B_1 = 20$ MHz and $B_2 = 50$ MHz (considered in Fig. 7) but also for the case $B_1 = 50$ MHz and $B_2 = 200$ MHz and the case $B_1 = 100$ MHz and $B_2 = 400$ MHz. As expected, the use of larger bandwidths results in a higher capacity. Moreover, it can also be noticed that increasing the bandwidths also reduces the distance at which the FR1 backup link starts being used more frequently, which determines a trade-off between capacity and usage of the FR1 backup link depending on the selected channel bandwidths.

VI. Conclusions

This work has proposed a dynamic hybrid FR1/FR2 transmission scheme with adaptive combining for improved reliability of wireless communications in mmWave bands. The obtained results demonstrate that the proposed scheme can achieve the same level of reliability (in terms of probability of outage and bit-error rate) as the dual-link transmission scheme where both links (FR1 and FR2) are used continuously, however with a significantly lower level of usage of the FR1 link, thus resulting in a more efficient usage of the available spectral resources. Moreover, the attained high level of link reliability is not obtained at the expense of the link capacity, which is indeed improved by the application of the proposed scheme. These findings suggest that the proposed scheme is a suitable technique to effectively meet the URLLC requirements for 5G/6G in a resource-efficient manner.

The study of a similar hybrid scheme at higher frequencies (e.g., main link in sub-THz bands supported by an mmWave backup link) and the analysis of the performance with a backup link shared among multiple users is suggested as future work.

References

[1] H. Chen, R. Abbas, P. Cheng, M. Shirvanimoghaddam, W. Hardjawana, W. Bao, Y. Li, and B. Vucetic, "Ultra-reliable low latency cellular networks: use cases, challenges and approaches," *IEEE Commun. Mag.*, vol. 56, no. 12, pp. 119–125, Dec. 2018.

[2] G. Pocovi, H. Shariatmadari, G. Berardinelli, K. Pedersen, J. Steiner, and Z. Li, "Achieving ultra-reliable low-latency communications: challenges and envisioned system enhancements," *IEEE Netw.*, vol. 32, no. 2, pp. 8–15, Mar. 2018.

[3] D. Feng, C. She, K. Ying, L. Lai, Z. Hou, T. Q. S. Quek, Y. Li, and B. Vucetic, "Toward ultrareliable low-latency communications: typical scenarios, possible solutions, and open issues," *IEEE Veh. Technol. Mag.*, vol. 14, no. 2, pp. 94–102, Jun. 2019.

[4] 3rd Generation Partnership Project, "Technical Specification Group Radio Access Network; Study on Scenarios and Requirements for Next Generation Access Technologies (Release 17)," 3GPP, Tech. Rep. 3GPP TR 38.913, Mar. 2022, v17.0.0.

[5] M. Bennis, M. Debbah, and H. V. Poor, "Ultrareliable and low-latency wireless communication: tail, risk, and scale," *Proc. IEEE*, vol. 106, no. 10, pp. 1834–1853, Oct. 2018.

[6] P. Popovski, J. J. Nielsen, C. Stefanovic, E. d. Carvalho, E. Strom, K. F. Trillingsgaard, A.-S. Bana, D. M. Kim, R. Kotaba, J. Park, and R. B. Sorensen, "Wireless access for ultra-reliable low-latency communication: principles and building blocks," *IEEE Netw.*, vol. 32, no. 2, pp. 16–23, Mar. 2018.

[7] P. Popovski, C. Stefanović, J. J. Nielsen, E. de Carvalho, M. Angjelichinoski, K. F. Trillingsgaard, and A.-S. Bana, "Wireless access in ultra-reliable low-latency communication (URLLC)," *IEEE Trans. Commun.*, vol. 67, no. 8, pp. 5783–5801, Aug. 2019.

[8] H. Ji, S. Park, J. Yeo, Y. Kim, J. Lee, and B. Shim, "Ultra-reliable and low-latency communications in 5G downlink: physical layer aspects," *IEEE Wireless Commun.*, vol. 25, no. 3, pp. 124–130, Jun. 2018.

[9] T.-K. Le, U. Salim, and F. Kaltenberger, "An overview of physical layer design for ultra-reliable low-latency communications in 3GPP Releases 15, 16, and 17," *IEEE Access*, vol. 9, pp. 433–444, Jan. 2021.

[10] H. Lee and Y.-C. Ko, "Physical layer enhancements for ultra-reliable low-latency communications in 5G New Radio systems," *IEEE Commun. Stand. Mag.*, vol. 5, no. 4, pp. 112–122, Dec. 2021.

[11] G. J. Sutton, J. Zeng, R. P. Liu, W. Ni, D. N. Nguyen, B. A. Jayawickrama, X. Huang, M. Abolhasan, Z. Zhang, E. Dutkiewicz, and T. Lv, "Enabling technologies for ultra-reliable and low latency communications: from PHY and MAC layer perspectives," *IEEE Commun. Surveys Tuts.*, vol. 21, no. 3, pp. 2488–2524, Third Quarter 2019.

[12] G. Pocovi, K. I. Pedersen, and P. Mogensen, "Joint link adaptation and scheduling for 5G ultra-reliable low-latency communications," *IEEE Access*, vol. 6, pp. 28 912–28 922, May 2018.

[13] C. She, C. Yang, and T. Q. S. Quek, "Joint uplink and downlink resource configuration for ultra-reliable and low-latency communications," *IEEE Trans. Commun.*, vol. 66, no. 5, pp. 2266–2280, May 2018.

[14] J. Cheng and C. Shen, "Relay-assisted uplink transmission design of URLLC packets," *IEEE Internet Things J.*, vol. 9, no. 19, pp. 18 839–18 853, Oct. 2022.

[15] S. Kurma, P. K. Sharma, S. Dhok, K. Singh, and C.-P. Li, "Adaptive AF/DF two-way relaying in FD multi-user URLLC system with user mobility," *IEEE Trans. Wireless Commun.*, vol. 21, no. 12, pp. 10 224–10 241, Dec. 2022.

[16] Y. Zhang, W. Tang, and Y. Liu, "Multi-cell grant-free uplink IoT networks with hard deadline services in URLLC," *IEEE Wireless Commun. Lett.*, vol. 11, no. 7, pp. 1448–1452, Jul. 2022.

[17] M. C. Lucas-Estañ and J. Gozalvez, "Sensing-based grant-free scheduling for ultra reliable low latency and deterministic beyond 5G networks," *IEEE Trans. Veh. Technol.*, vol. 71, no. 4, pp. 4171–4183, Apr. 2022.

[18] K. Jiang, H. Zhou, X. Chen, and H. Zhang, "Mobile edge computing for ultra-reliable and low-latency communications," *IEEE Commun. Stand. Mag.*, vol. 5, no. 2, pp. 68–75, Jun. 2021.

[19] D. Van Huynh, S. R. Khosravirad, A. Masaracchia, O. A. Dobre, and T. Q. Duong, "Edge intelligence-based ultra-reliable and low-latency communications for digital twin-enabled metaverse," *IEEE Wireless Commun. Lett.*, vol. 11, no. 8, pp. 1733–1737, Aug. 2022.

[20] B. Kharel, O. L. A. López, N. H. Mahmood, H. Alves, and M. Latva-Aho, "Fog-RAN enabled multi-connectivity and multi-cell scheduling framework for ultra-reliable low latency communication," *IEEE Access*, vol. 10, pp. 7059–7072, Jan. 2022.

[21] Y. Wang, W. Chen, and H. V. Poor, "Ultra-reliable and low-latency wireless communications in the high SNR regime: a cross-layer tradeoff," *IEEE Trans. Commun.*, vol. 70, no. 1, pp. 149–162, Jan. 2022.

[22] G. Pocovi, T. Kolding, and K. I. Pedersen, "On the cost of achieving downlink ultra-reliable low-latency communications in 5G networks," *IEEE Access*, vol. 10, pp. 29 506–29 513, Mar. 2022.

[23] A. Anand, G. de Veciana, and S. Shakkottai, "Joint scheduling of URLLC and eMBB traffic in 5G wireless networks," *IEEE/ACM Trans. Netw.*, vol. 28, no. 2, pp. 477–490, Apr. 2020.

[24] Y. Prathyusha and T.-L. Sheu, "Coordinated resource allocations for eMBB and URLLC in 5G communication networks," *IEEE Trans. Veh. Technol.*, vol. 71, no. 8, pp. 8717–8728, Aug. 2022.

[25] M. Alsenwi, N. H. Tran, M. Bennis, S. R. Pandey, A. K. Bairagi, and C. S. Hong, "Intelligent resource slicing for eMBB and URLLC coexistence in 5G and beyond: a deep reinforcement learning based approach," *IEEE Trans. Wireless Commun.*, vol. 20, no. 7, pp. 4585–460, Jul. 2021.

[26] Y. Zhao, X. Chi, L. Qian, Y. Zhu, and F. Hou, "Resource allocation and slicing puncture in cellular networks with eMBB and URLLC terminals coexistence," *IEEE Internet Things J.*, vol. 9, no. 19, pp. 18 431–18 444, Oct. 2022.

[27] M.-T. Suer, C. Thein, H. Tchouankem, and L. Wolf, "Multi-connectivity as an enabler for reliable low latency communications – an overview," *IEEE Commun. Surveys Tuts.*, vol. 22, no. 1, pp. 156–169, First Quarter 2020.

[28] 3rd Generation Partnership Project, "Technical Specification Group Radio Access Network; NR; User Equipment (UE) radio transmission and reception; Part 1: Range 1 Standalone (Release 17)," 3GPP, Tech. Rep. 3GPP TS 38.101-1, Mar. 2022, v17.5.0.

[29] ——, "Technical Specification Group Radio Access Network; NR; User Equipment (UE) radio transmission and reception; Part 2: Range 2 Standalone (Release 17)," 3GPP, Tech. Rep. 3GPP TS 38.101-2, Mar. 2022, v17.5.0.

[30] Z. Pi and F. Khan, "An introduction to millimeter-wave mobile broadband systems," *IEEE Commun. Mag.*, vol. 49, no. 6, pp. 101–107, Jun. 2011.

[31] I. A. Hemadeh, K. Satyanarayana, M. El-Hajjar, and L. Hanzo, "Millimeter-wave communications: physical channel models, design considerations, antenna constructions, and link-budget," *IEEE Commun. Surveys Tuts.*, vol. 20, no. 2, pp. 870–913, Second Quarter 2018.

[32] T. S. Rappaport, R. W. Heath, R. C. Daniels, and J. N. Murdock, *Millimeter wave wireless communication*. New Jersey, USA: Prentice-Hall, 2015.

[33] D. Ohmann, A. Awada, I. Viering, M. Simsek, and G. P. Fettweis, "Diversity trade-offs and joint coding schemes for highly reliable wireless transmissions," in *Proceedings of the 84th IEEE Vehicular Technology Conference (VTC-Fall 2016)*, Sep. 2016, pp. 1–6.

[34] M. K. Simon and M.-S. Alouini, *Digital communications over fading channels*, 2nd ed. Wiley-IEEE Pres, 2005.

[35] G. L. Stüber, *Principles of mobile communciation*, 4th ed. Springer, 2017.

[36] J. M. Romero-Jerez, F. J. Lopez-Martinez, J. F. Paris, and A. J. Goldsmith, "The fluctuating two-ray fading model: statistical characterization and performance analysis," *IEEE Trans. Wireless Commun.*, vol. 16, no. 7, pp. 4420–4432, Jul. 2017.

[37] J. Zhang, W. Zeng, X. Li, Q. Sun, and K. P. Peppas, "New results on the fluctuating two-ray model with arbitrary fading parameters and its applications," *IEEE Trans. Veh. Technol.*, vol. 67, no. 3, pp. 2766–2770, Mar. 2018.

[38] I. Gradshteyn and I. Ryzhik, *Table of integrals, series, and products*, 7th ed. London, UK: Academic Press, 2007.

[39] M. López-Benítez and J. Zhang, "Comments and corrections to new results on the fluctuating two-ray model with arbitrary fading parameters and its applications," *IEEE Trans. Veh. Technol.*, vol. 70, no. 2, pp. 1938–1940, Feb. 2021.

[40] A. Papoulis and S. U. Pillai, *Probability, random variables and stochastic processes*, 4th ed. McGraw Hill, 2001.

[41] T. K. Vu, M. Bennis, M. Debbah, M. Latva-aho, and C. S. Hong, "Ultra-reliable communication in 5G mmWave networks: a risk-sensitive approach," *IEEE Commun. Lett.*, vol. 22, no. 4, pp. 708–711, Apr. 2018.

[42] A. Wolf, P. Schulz, M. Dörpinghaus, J. C. S. Santos Filho, and G. Fettweis, "How reliable and capable is multi-connectivity?" *IEEE Trans. Commun.*, vol. 67, no. 2, pp. 1506–1520, Feb. 2019.

[43] A. H. Wojnar, "Unknown bounds on performance in Nakagami channels," *IEEE Trans. Commun.*, vol. 34, no. 1, pp. 22–24, Jan. 1986.

[44] E. D. Vagenas, P. Karadimas, and S. A. Kotsopoulos, "Ergodic capacity for the SIMO Nakagami-m channel," *EURASIP J. Wireless Commun. Netw.*, vol. 2009, no. 802067, pp. 1–9, Aug. 2009.

[45] A. I. Sulyman, A. T. Nassar, M. K. Samimi, G. R. MacCartney, T. S. Rappaport, and A. Alsanie, "Radio propagation path loss models for 5G cellular networks in the 28 GHz and 38 GHz millimeter-wave bands," *IEEE Commun. Mag.*, vol. 52, no. 9, pp. 78–86, Sep. 2014.

[46] M. K. Samimi, T. S. Rappaport, and G. R. MacCartney, "Probabilistic omnidirectional path loss models for millimeter-wave outdoor communications," *IEEE Wireless Commun. Lett.*, vol. 4, no. 4, pp. 357–360, Aug. 2015.